RSC Advances

PAPER

View Article Online
View Journal | View Issue

Cite this: *RSC Adv.*, 2014, **4**, 30274

Syntheses, structures, and luminescence properties of four metal–organic polymers with undocumented topologies constructed from 3,5-bis((4′-carboxylbenzyl)oxy)benzoate ligand†

Xiutang Zhang,*[ab] Liming Fan,[ab] Weikuo Song,[a] Weiliu Fan,[b] Liming Sun[b] and Xian Zhao*[b]

Received 19th May 2014
Accepted 30th June 2014

DOI: 10.1039/c4ra04707a

www.rsc.org/advances

Solvothermal reactions of one semirigid tricarboxylic acid and transition metal cations in the absence or presence of 1,4-bis(1*H*-imidazol-4-yl)benzene (1,4-bib) afford four coordination polymers, namely, $[Cd(Hbcb)]_n$ (**1**), and $[M(Hbcb)(1,4\text{-bib})]_n$ (M = Cd (**2**), Mn (**3**), Fe (**4**)) (H_3bcb = 3,5-bis((4′-carboxylbenzyl)-oxy)benzoic acid). Their structures have been determined by single-crystal X-ray diffraction analyses and further characterized by elemental analyses, IR spectra, powder X-ray diffraction (PXRD), and thermogravimetric (TG) analyses. Structural analysis revealed that complex **1** exhibits an intriguing $[Cd(COO)_2]_n$ tube-like chain based 3D framework with unprecedented 6-connected ($4^8\cdot6^7$) topology. Complexes **2–4** show isomorphism and show new 3D (3,5)-connected frameworks with the point Schläfli symbol of $(4\cdot6\cdot8)(4\cdot6^4\cdot8^5)$ based on the $[M(COO)]_n$ chain. Moreover, the photoluminescence properties of **1** and **2** have been investigated in the solid state at room temperature.

Introduction

The rational design and construction of functional materials based on organic ligands has been a subject of growing interest in the past two decades due to their exceptionally artistic topologies and tremendous potential applications, such as gas adsorption and separation, ion exchange, nonlinear optics, heterogeneous catalysis, and luminescence.[1–4] These intriguing properties and excellent applications are mostly attributed to the distinct architecture and composition of the metal–organic polymers.[5] It is well-known that the experimental conditions during the self-assembly process play a vital role on the growth of the single crystals, such as temperature, metal ions, template, pH value, counteranion, reaction period, concentrations of the raw materials, and so on.[6,7] Among these factors, tactical design or selection of the characteristic organic ligands according to their length, rigidly, and functional groups was proved to be one efficient route for achieving expected MOFs.[8,9]

However, it is still one tremendous challenge to design and synthesize such crystal materials for coordination chemistry researchers, although considerable progress in the practical and theoretic approaches have been achieved.[10,11] The most common strategy is one-pot reaction of metal ions and selected organic ligands by serendipitous self-assembly although it is

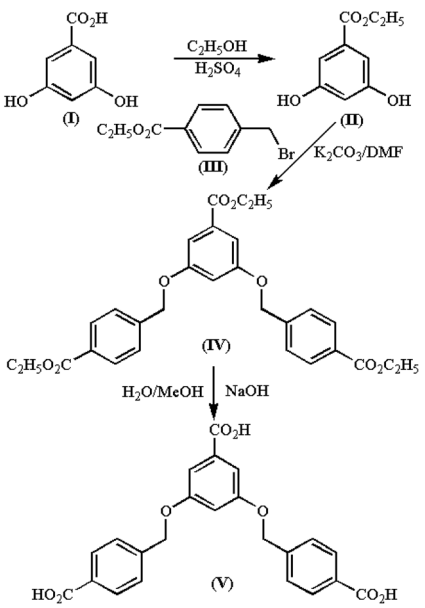

Scheme 1 The scheme for the synthesis of H_3bcb.

[a]*Advanced Material Institute of Research, College of Chemistry and Chemical Engineering, Qilu Normal University, Jinan 250013, China. E-mail: xiutangzhang@163.com*

[b]*State Key Laboratory of Crystal Materials, Shandong University, Jinan 250100, China. E-mail: zhaoxian@icm.sdu.edu.cn*

† Electronic supplementary information (ESI) available: Additional Figures, powder X-ray diffraction (PXRD) patterns, thermogravimetric analysis (TGA) and IR spectra for **1–4**. X-ray crystallographic data, CCDC 986465–986468 for **1–4**. For ESI and crystallographic data in CIF or other electronic format see DOI: 10.1039/c4ra04707a

impossible to predict the final crystal structure. This strategy has been proved effective and were widely applied in many systems.[12,13]

Recent study on coordination assemblies using biphenyl-3,4′,5-tricarboxylic acid (H_3BPT) and bis(imidazole) linkers states a reliable strategy for obtaining new topological prototypes of coordination nets.[13c] Also, a minor change of the carboxylate building blocks may be applied to realize good structural control of the resulting coordination polymers. Thus, these considerations inspired us to explore novel metal–organic coordination architectures with the designed semirigid 3,5-bis((4′-arboxylbenzyl)oxy)benzoic acid (H_3bcb, Scheme 1). Compared with the rigid H_3BPT, H_3bcb is a more flexible and longer ligand, which owns the followed intriguing characters: (i) three carboxyl groups may be partially or completely deprotonated, resulting in rich coordination modes and interesting topologies with higher dimensionalities, (ii) three benzoate groups separated could form different dihedral angles through the rotation of –O–C– groups, thus it may coordinate metal centers in different orientations. These characters may lead to helical structures, cavities, interpenetration, and other novel motifs with extraordinary topologies. Taking account of the above viewpoints, recently we began to assemble polymeric complexes with H_3bcb and transitional metal ions and anticipated the rich structural features stored in H_3bcb will induce new metal–organic structures.

In this paper, four new complexes with interestingly topologies have been synthesized, namely, $[Cd(Hbcb)]_n$ (**1**), and $[M(Hbcb)(1,4\text{-bib})]_n$ (M = Cd (**2**), Mn (**3**), Fe (**4**)). Their structures and properties were measured and identified by physical methods. Due to the excellent coordination abilities of H_3bcb, compounds **1–4** exhibit 3D frameworks, built from the intriguing 1D metal-carboxyl chains, exhibiting undocumented topologies: 6-connected $(4^8\cdot6^7)$ for **1** and (3,5)-connected $(4\cdot6\cdot8)(4\cdot6^4\cdot8^5)$ for **2–4**.

Experimental section

Materials and physical measurements

All chemicals were purchased from Jinan Henghua Sci. & Tec. Co. Ltd. without further purification. IR spectra were measured on a NEXUS 670 FTIR spectrometer at the range of 600–4000 cm^{-1}. Elemental analyses were carried out on a CE instruments EA 1110 elemental analyzer. X-ray powder diffractions were measured on a Panalytical X-Pert pro diffractometer with Cu-Kα radiation. Thermogravimetric analyses (TGA) were performed under air condition from room temperature to 800 °C with a heating rate of 10 °C min^{-1} on Perkin-Elmer TGA-7 thermogravimetric analyzer. Fluorescence spectra were performed on a Hitachi F-4500 fluorescence spectrophotometer at room temperature.

Synthesis of 3,5-bis((4′-carboxylbenzyl)oxy)benzoic acid (H_3bcb) (Scheme 1)

Synthesis of ethyl 3,5-dihydroxybenzoate (II). The mixture of 3,5-dihydroxybenzoic acid (0.1 mol, 15.4 g) and 10 mL concentrated H_2SO_4 in 500 mL ethanol was refluxed for 12 hours, and then poured into 500 mL H_2O. White solid was filtrated and recrystallized from methanol with the yield of 85%. Anal. (%) calcd for $C_9H_{10}O_4$: C, 59.34; H, 5.53. Found: C, 59.16; H, 5.40.

Synthesis of ethyl 4-bromomethylbenzoate (III). The mixture of 4-(bromomethyl)benzonitrile (0.1 mol, 19.6 g) and 10 mL concentrated H_2SO_4 in 500 mL ethanol was refluxed for 3 days, and then poured into 500 mL H_2O. Ethyl acetate was used to extract for three times. White solid was obtained after vacuum concentration with the yield of 56%. Anal. (%) calcd for $C_{10}H_{11}BrO_2$: C, 49.41; H, 4.56. Found: C, 49.32; H, 4.43.

Synthesis of ethyl 3,5-bi(4-cyanophenoxy)benzoate (IV). The mixture of **II** (0.05 mol, 9.1 g), **III** (0.10 mol, 24.2 g), and potassium carbonate (0.1 mmol, 13.8 g) in 500 mL DMSO was refluxed at 120 °C for one week and then poured into 2000 mL H_2O. The obtained solid was recrystallized from methanol and purified by silica gel chromatography with a eluting mixture of chloroform and acetone (2 : 1, v/v), with 36% yield. Anal. (%) calcd for $C_{29}H_{30}O_8$: C, 68.76; H, 5.97. Found: C, 68.58; H, 5.79.

Synthesis of 3,5-bis((4′-carboxylbenzyl)oxy)benzoic acid (H_3bcb) (V). The mixture of **IV** (0.05 mol, 25.3 g) and NaOH (0.2 mol, 8.0 g) in the mixed solvent of EtOH (500 mL) and H_2O (500 mL) was refluxed at 75 °C for one day and filtrated. The filtrated solution was adjusted to pH = 3 to result in white solid. Recrystallization was applied in DMSO with the yield of 72%. EI-MS: m/z $[M-H]^-$, 421.1 (calcd for $C_{23}H_{18}O_8$, 422.1). Anal. (%) calcd for $C_{23}H_{18}O_8$: C, 65.40; H, 4.30. Found: C, 65.21; H, 4.13.

Synthesis of $[Cd(Hbcb)]_n$ (1). A mixture of H_3bcb (0.20 mmol, 0.083 g), $3CdSO_4\cdot8H_2O$ (0.13 mmol, 0.103 g), NaOH (0.10 mmol, 0.004 g) and 12 mL H_2O was placed in a Teflon-lined stainless steel vessel, heated to 170 °C for 3 days, followed by slow cooling (a descent rate of 10 °C per h) to room temperature. Light yellow block crystals of **1** were obtained. Yield of 37% (based on Cd). Anal. (%) calcd for $C_{23}H_{16}CdO_8$: C, 51.85; H, 3.03. Found: C, 52.17; H, 3.12. IR (KBr pellet, cm^{-1}): 3039 (m), 2642 (w), 1683 (s), 1592 (vs), 1549 (vs), 1360 (vs), 1247 (s), 1060 (m), 824 (m), 770 (m), 720 (w).

Synthesis of $[Cd(Hbcb)(1,4\text{-bib})]_n$ (2). A mixture of H_3bcb (0.2 mmol, 0.083 g), 1,4-bib (0.20 mmol, 0.042 g), $3CdSO_4\cdot8H_2O$ (0.13 mmol, 0.103 g), NaOH (0.10 mmol, 0.004 g), and 12 mL H_2O was placed in a Teflon-lined stainless steel vessel, heated to 170 °C for 3 days, followed by slow cooling (a descent rate of 10 °C per h) to room temperature. Colourless block crystals of **2** were obtained. Yield of 57% (based on Cd). Anal. (%) calcd for $C_{35}H_{26}CdN_4O_8$: C, 56.59; H, 3.53; N, 7.54. Found: C, 56.30; H, 3.69; N, 7.82. IR (KBr pellet, cm^{-1}): 3134 (m), 2596 (m), 1692 (s), 1593 (vs), 1527 (vs), 1371 (s), 1154 (s), 1049 (m), 834 (m), 753 (m).

Synthesis of $[Mn(Hbcb)(1,4\text{-bib})]_n$ (3). The same synthetic procedure as for **2** was used except that $3CdSO_4\cdot8H_2O$ was replaced by $MnSO_4\cdot H_2O$ (0.40 mmol, 0.068 g), giving colourless block crystals. Yield of 53% (based on Mn). Anal. (%) calcd for $C_{35}H_{26}MnN_4O_8$: C, 61.32; H, 3.82; N, 8.17. Found: C, 61.30; H, 4.03; N, 8.02. IR (KBr pellet, cm^{-1}): 3125 (m), 2876 (w), 1691 (s), 1595 (vs), 1442 (vs), 1371 (vs), 1237 (m), 1062 (s), 834 (m), 756 (m).

Synthesis of [Fe(Hbcb)(1,4-bib)]$_n$ (4). The same synthetic procedure as for **2** was used except that $3CdSO_4 \cdot 8H_2O$ was replaced by $FeSO_4 \cdot 7H_2O$ (0.40 mmol, 0.112 g), giving orange block crystals. Yield of 62% (based on Fe). Anal. (%) calcd for $C_{35}H_{26}FeN_4O_8$: C, 61.24; H, 3.82; N, 8.16. Found: C, 61.37; H, 3.96; N, 8.45. IR (KBr pellet, cm^{-1}): 3145 (m), 2877 (m), 1692 (s), 1595 (vs), 1406 (vs), 1371 (vs), 1248 (s), 1050 (s), 835 (m), 754 (m).

X-ray crystallography. Intensity data collection was carried out on a Siemens SMART diffractometer equipped with a CCD detector using Mo-Kα monochromatized radiation ($\lambda = 0.71073$ Å). The absorption correction was based on multiple and symmetry-equivalent reflections in the data set using the SADABS program based on the method of Blessing. The structures were solved by direct methods and refined by full-matrix least-squares using the SHELXTL package.[14] All non-hydrogen atoms were refined anisotropically. Hydrogen atoms were generated geometrically with fixed isotropic thermal parameters. Crystallographic data for complexes **1–4** are given in Table 1. Selected bond lengths and angles for **1–4** are listed in Table 2.† Topological analysis of the coordination networks of **1–4** was performed with the program package TOPOS.[15]

Result and discussion

Synthesis and characterization

Complexes **1–4** were prepared from the solvothermal reaction of H_3bcb and related transitional metal salts in similar reaction conditions. Other transition metal salts also were used to react with H_3bcb under similar reaction condition of complex **1**, unfortunately we just obtained some unknown powder substance in the end. The ancillary co-ligands were introduced to adjust the final structure with mixed ligands strategy. The linear 1,4-bib (1,4-bis(1*H*-imidazol-4-yl)benzene) as well as some other bridging imidazole linkers (V-shaped 1,3-bis(1*H*-imidazol-4-yl)benzene ligand, the flexible 1,3-bis(imidazol-1-ylmethyl)-benzene ligand, 1,4-bis(imidazol-1-ylmethyl)benzene ligand, and longer 4,4′-bis(imidazol-1-yl)biphenyl ligand) have been selected as co-ligands to modify the network, but only three 1,4-bib based complexes were constructed, which might attribute to the coordination preference of H_3bcb. Besides, the 1,4-bib ligand can separated the neighbouring cations with a proper distance. The solid state of **1–4** are stable upon exposure to air.

Structural description of [Cd(Hbcb)]$_n$ (1)

Single-crystal X-ray diffraction analysis revealed that complex **1** crystallizes in the orthorhombic $Pna2_1$ space group. As shown in Fig. 1, the asymmetric unit of **1** contains one crystallographically independent Cd^{II} anion and one partly deprotonated $Hbcb^{2-}$ ligand. Each Cd^{II} ion is hexa-coordinated and surrounded by six carboxyl oxygen atoms from six individual $Hbcb^{2-}$ ligands, forming octahedral coordination geometry. The Cd–O bond distances range from 2.199(6) to 2.371(3) Å, and the dihedral angles around Cd^{II} are in the range of 80.90(9)–174.85(9)°.

The ligand of $Hbcb^{2-}$ acts as one μ_6 node to coordinate with six Cd^{II} ions, in which the protonated carboxyl group adopts monodentate μ_1-η^1:η^0 coordination mode and the two deprotonated carboxyl groups adopt bridging μ_2-η^1:η^1 and μ_3-η^2:η^1 modes, respectively (Mode I, Scheme 2). It is noteworthy that the Cd^{II} ions are linked by the carboxyl groups to form an unprecedented 1D tube-like $[Cd(COO)_2]_n$ chain, with the diameter being *ca.* 2.04 Å. The nearest Cd···Cd distances are 3.824 and 4.696 Å, respectively (Fig. 2). Furthermore, three parallel

Table 1 Crystal data for **1–4**

Compound	1	2	3	4
Empirical formula	$C_{23}H_{16}CdO_8$	$C_{35}H_{26}CdN_4O_8$	$C_{35}H_{26}MnN_4O_8$	$C_{35}H_{26}FeN_4O_8$
Formula weight	532.76	743.00	685.54	686.45
Crystal system	Orthorhombic	Orthorhombic	Orthorhombic	Orthorhombic
Space group	*Pna*2$_1$	*Pbcn*	*Pbcn*	*Pbcn*
a (Å)	19.0064(19)	27.0432(17)	26.780(2)	26.4977(19)
b (Å)	24.517(2)	8.0754(5)	8.1675(7)	8.1948(6)
c (Å)	4.6956(5)	27.1949(17)	26.928(2)	26.8556(6)
α (°)	90.00	90.00	90.00	90.00
β (°)	90.00	90.00	90.00	90.00
γ (°)	90.00	90.00	90.00	90.00
V (Å^3)	2188.0(4)	5938.9(6)	5889.9(9)	5831.5(6)
Z	4	8	8	8
D_{calcd} (Mg m^{-3})	1.617	1.662	1.546	1.564
μ (mm^{-1})	1.045	0.800	0.513	0.583
θ range	1.36–25.00	1.68–25.00	1.69–25.00	1.70–25.10
Reflections collected	11 049	29 097	28 793	28 865
Data/parameters	3730/290	5239/434	5188/434	5139/434
F (000)	1064	3008	2824	2832
T (K)	293(2)	296(2)	293(2)	296(2)
R_{int}	0.0364	0.0573	0.1282	0.0668
R_1 (wR_2) [$I > 2\sigma(I)$]	$R_1 = 0.0680$ w$R_2 = 0.2271$	$R_1 = 0.0309$ w$R_2 = 0.0538$	$R_1 = 0.0488$ w$R_2 = 0.0987$	$R_1 = 0.0406$ w$R_2 = 0.0905$
R_1 (wR_2) (all data)	$R_1 = 0.0778$ w$R_2 = 0.2400$	$R_1 = 0.0507$ w$R_2 = 0.0577$	$R_1 = 0.0972$ w$R_2 = 0.1088$	$R_1 = 0.0731$ w$R_2 = 0.0984$
Gof	1.002	1.001	1.007	1.007

$R_1 = \Sigma||F_o| - |F_c||/\Sigma|F_o|$, $wR_2 = [\Sigma w(F_o^2 - F_c^2)^2]/\Sigma w(F_o^2)^2]^{1/2}$

Table 2 Selected bond lengths (Å) and angles (°) for **1–4**

Complex 1							
Cd(1)–O(5)$^{\#1}$	2.207(8)	Cd(1)–O(6)$^{\#2}$	2.257(6)	Cd(1)–O(2)	2.28(2)	Cd(1)–O(1)$^{\#3}$	2.305(7)
Cd(1)–O(7)$^{\#4}$	2.341(7)	Cd(1)–O(6)$^{\#5}$	2.375(8)	O(5)$^{\#1}$–Cd(1)–O(6)$^{\#2}$	103.1(3)	O(5)$^{\#1}$–Cd(1)–O(2)	165.8(5)
O(6)$^{\#2}$–Cd(1)–O(2)	90.2(6)	O(5)$^{\#1}$–Cd(1)–O(1)$^{\#3}$	95.8(3)	O(6)$^{\#2}$–Cd(1)–O(1)$^{\#3}$	98.8(3)	O(2)–Cd(1)–O(1)$^{\#3}$	86.9(5)
O(5)$^{\#1}$–Cd(1)–O(7)$^{\#4}$	81.2(3)	O(6)$^{\#2}$–Cd(1)–O(7)$^{\#4}$	174.9(3)	O(2)–Cd(1)–O(7)$^{\#4}$	85.3(6)	O(1)$^{\#3}$–Cd(1)–O(7)$^{\#4}$	83.3(3)
O(5)$^{\#1}$–Cd(1)–O(6)$^{\#5}$	87.4(3)	O(6)$^{\#2}$–Cd(1)–O(6)$^{\#5}$	92.92(18)	O(2)–Cd(1)–O(6)$^{\#5}$	86.9(5)	O(1)$^{\#3}$–Cd(1)–O(6)$^{\#5}$	166.8(3)
O(7)$^{\#4}$–Cd(1)–O(6)$^{\#5}$	84.6(2)						
Symmetry code: #1 $-x + 1/2, y - 1/2, z + 3/2$; #2 $x + 1/2, -y + 3/2, z+1$; #3 $x, y, z + 1$; #4 $x - 1/2, -y + 3/2, z - 1$; #5 $-x + 1/2, y - 1/2, z + 1/2$							
Complex 2							
Cd(1)–O(8)$^{\#3}$	2.186(2)	Cd(1)–N(1)	2.250(2)	Cd(1)–O(1)	2.282(2)	Cd(1)–N(3)	2.305(2)
Cd(1)–O(2)$^{\#4}$	2.323(2)	O(8)$^{\#3}$–Cd(1)–N(1)	98.11(9)	O(8)$^{\#3}$–Cd(1)–O(1)	108.76(8)	N(1)–Cd(1)–O(1)	94.34(8)
O(8)$^{\#3}$–Cd(1)–N(3)	88.68(9)	N(1)–Cd(1)–N(3)	171.49(9)	O(1)–Cd(1)–N(3)	88.26(8)	O(8)$^{\#3}$–Cd(1)–O(2)$^{\#4}$	154.40(8)
N(1)–Cd(1)–O(2)$^{\#4}$	93.59(9)	O(1)–Cd(1)–O(2)$^{\#4}$	92.87(7)	N(3)–Cd(1)–O(2)$^{\#4}$	78.17(8)		
Symmetry code: #3 $-x + 1, -y - 1, -z + 2$; #4 $-x + 3/2, y - 1/2, z$							
Complex 3							
Mn(1)–O(4)$^{\#3}$	2.069(3)	Mn(1)–O(8)$^{\#4}$	2.107(2)	Mn(1)–O(7)	2.180(2)	Mn(1)–N(1)	2.193(3)
Mn(1)–N(3)	2.237(3)	O(4)$^{\#3}$–Mn(1)–O(8)$^{\#4}$	108.68(11)	O(4)$^{\#3}$–Mn(1)–O(7)	151.04(11)	O(8)$^{\#4}$–Mn(1)–O(7)	98.19(10)
O(4)$^{\#3}$–Mn(1)–N(1)	95.76(11)	O(8)$^{\#4}$–Mn(1)–N(1)	95.68(11)	O(7)–Mn(1)–N(1)	92.04(11)	O(4)$^{\#3}$–Mn(1)–N(3)	89.13(11)
O(8)$^{\#4}$–Mn(1)–N(3)	90.45(10)	O(7)–Mn(1)–N(3)	79.86(10)	N(1)–Mn(1)–N(3)	170.49(12)		
Symmetry codes: #3 $x + 1/2, -y + 1/2, -z + 1$; #4 $-x + 1/2, y + 1/2, z$							
Complex 4							
Fe(1)–O(8)$^{\#3}$	1.996(2)	Fe(1)–O(2)	2.0788(19)	Fe(1)–O(1)$^{\#4}$	2.095(2)	Fe(1)–N(3)	2.153(2)
Fe(1)–N(1)	2.199(2)	O(8)$^{\#3}$–Fe(1)–O(2)	151.13(9)	O(8)$^{\#3}$–Fe(1)–O(1)$^{\#4}$	109.85(9)	O(2)–Fe(1)–O(1)$^{\#4}$	97.44(8)
O(8)$^{\#3}$–Fe(1)–N(3)	95.50(9)	O(2)–Fe(1)–N(3)	92.38(9)	O(1)$^{\#4}$–Fe(1)–N(3)	92.68(9)	O(8)$^{\#3}$–Fe(1)–N(1)	89.94(9)
O(2)–Fe(1)–N(1)	80.90(8)	O(1)$^{\#4}$–Fe(1)–N(1)	89.30(8)	N(3)–Fe(1)–N(1)	173.19(9)		
Symmetry codes: #3 $x + 1/2, -y + 3/2, -z + 2$; #4 $-x + 1/2, y - 1/2, z$							

$[Cd(COO)_2]_n$ chains are connected by three carboxyl groups of one $Hbcbb^{2-}$ linker, leaving one 3D $[Cd(Hbcb)]_n$ framework (Fig. 3). The dihedral angles between two phenyl rings and central phenyl ring in one $Hbcb^{2-}$ are 27.5(3), and 82.5(3)°, respectively. And the one between two phenyl rings is 66.6(6)°. Those dihedral angles indicate that the $Hbcbb^{2-}$ is extremely unsymmetrical and distorted during the self-assembly process. Besides, the void volume in **1** is 14.7% of the crystal volume (321.3 out of the 2188.1 Å^3 unit cell volume), calculated by PLATON.[16]

To better understand the structure of **1**, the topological analysis approach is employed. From the topological point of view, both $Hbcb^{2-}$ ligands and Cd^{II} act as 6-connected nodes, giving rise to an unprecedented 6-connected net with the Schläfli symbol of $(4^8 \cdot 6^7)$, shown in Fig. 4. To our knowledge, this topology has never been reported before.

Structural description of $[M(Hbcb)(1,4\text{-bib})]_n$ (M = Cd (2), Mn (3), Fe (4))

With the ancillary ligand of 1,4-bib being employed in the reaction, part of coordination geometry around metal center were occupied by nitrogen atoms from imidazole rings in 1,4-bib ligand. The stereospecific blockade of 1,4-bib resulted in distorted trigonal bipyramidal coordination geometries around metal cations in **2–4**.

The single-crystal X-ray diffraction analyses reveal that complexes **2–4** are isomorphous and crystallize in the orthorhombic *Pbcn* space group, herein only the structure of **2** will be discussed as a representation. As shown in Fig. 5, there are one crystallographically independent Cd^{II} ion, one $Hbcb^{2-}$ ligand, and one 1,4-bib ligand in the asymmetric unit. Each Cd^{II} center is penta-coordinated by two nitrogen atoms from two 1,4-bib ligands [Cd(1)–N(1) = 2.250(2), and Cd(1)–N(3) = 2.305(2) Å] and three oxygen atoms from three $Hbcb^{2-}$ ligands [Cd(1)–O(1) = 2.282(2), Cd(1)–O(2) = 2.323(2), and Cd(1)–O(8) = 2.186(2) Å], forming a distorted trigonal bipyramidal coordination geometry.

Although the ligand of H_3bcb is also partly deprotonated, $Hbcb^{2-}$ in complex **2** act as one μ_3 node to coordinate with three Cd^{II} ions, in which two deprotonated carboxyl groups adopt μ_2-η^2:η^1 and μ_1-η^1:η^0 coordination modes (Mode II), respectively, shown in Scheme 2. The dihedral angles between the two benzyl rings and central phenyl ring in $Hbcbb^{2-}$ are 62.6(5) and 89.9(3)°, respectively, and the one between two phenyl rings is 62.7(8)°. The dihedral angles are slightly different for compounds **2–4**: 63.2(6), 88.5(9), and 63.2(2)° for complex **3**; and 64.3(7), 87.1(9), and 63.3(6)° for complex **4**.

Each Cd^{II} ions are linked by μ_2-η^2:η^1 carboxyl groups to form a 1D $[Cd(COO)]_n$ chain, with the Cd···Cd distance being 4.298 Å (Fig. S1†). And then the $Hbcbb^{2-}$ anions act as bridging pillars, further expanded the 1D $[Cd(COO)]_n$ chains to a 2D $[Cd(Hbcb)]_n$ sheet along the *ab* plane (Fig. S2†). Besides, the ancillary 1,4-bib

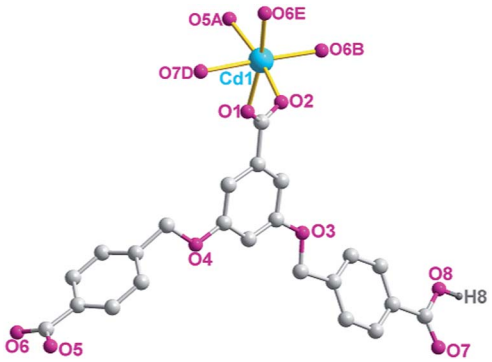

Fig. 1 ORTEP representation of **1** showing the local coordination environment around Cd^{II} center. (Symmetry codes: (A) 0.5−*x*, −0.5 + *y*, 1.5 + *z*; (B) 0.5 + *x*, 1.5−*y*, 1 + *z*; (D) −0.5 + *x*, 1.5−*y*, −1 + *z*; (E) 0.5−*x*, −0.5 + *y*, 1.5 + *z*.).

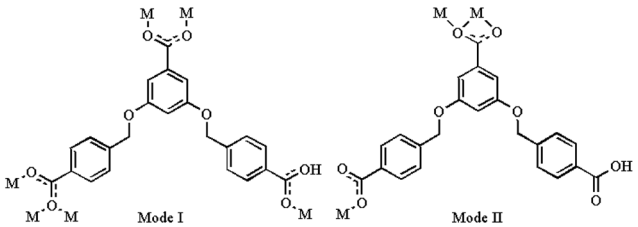

Scheme 2 The coordinaion modes of H_3bcb in complexes **1**–**4**.

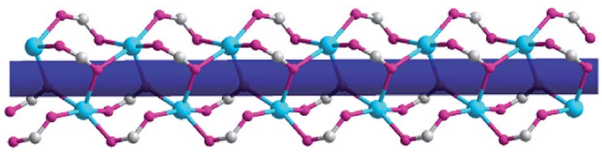

Fig. 2 The intriguing 1D $[Cd(COO)_2]_n$ tube-like chain in complex **1**.

as bridging linkers connected with the metal centres, successfully constructed a linear $[Cd(1,4\text{-bib})]_n$ chain along *c* direction. The linear $[Cd(1,4\text{-bib})]_n$ chains pulling the neighbouring 2D $[Cd(Hbcb)]_n$ sheets together, finally generated a 3D framework (Fig. 6).

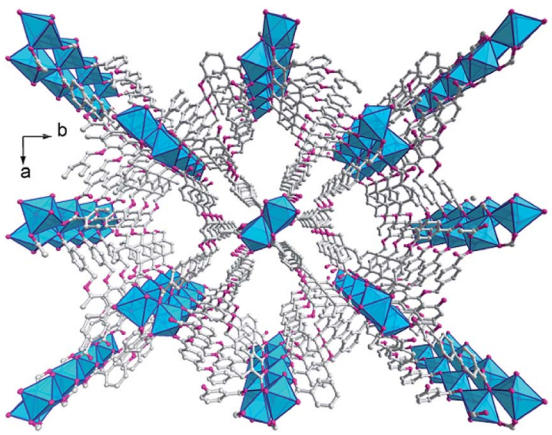

Fig. 3 The 3D frameworks view along *c* axis in complex **1**.

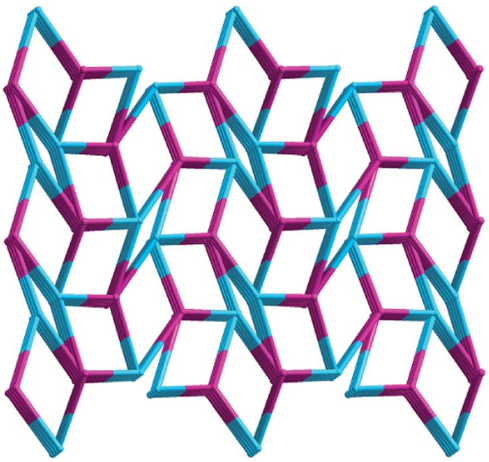

Fig. 4 Schematic view of the novel 6-connected $(4^8\cdot6^7)$ topology of **1**.

From the viewpoint of structural topology, the overall frameworks of complex **2** can be defined as a new binodal (3,5)-connected nets with the Schläfli symbol of $(4\cdot6\cdot8)(4\cdot6^4\cdot8^5)$ by denoting Cd^{II} and $Hbcb^{2-}$ as five- and three-connected nodes, the bridging 1,4-bib ligands as linkers, respectively (Fig. 7).

Structural comparisons

As shown in the Scheme 2, the H_3bcb exhibits two different coordination modes. Although both two coordination modes are partly deprotonated, the one in complex **1** adopts μ_6-η^1:η^0-η^1:η^1-η^1:η^2 coordination mode (Mode I), act as a trifunctional ligand, compared with bifunctional bridging $Hbcb^{2-}$ linker with μ_3-η^1:η^2-η^0:η^1 coordination mode (Mode II). The three carboxyl groups of trifunctional $Hbcb^{2-}$ ligated with Cd^{II} ions with monodentate μ_1-η^1:η^0, bridging μ_2-η^1:η^1, and bridging μ_3-η^1:η^2 carboxyl groups, obtained an interestingly 1D $[Cd(COO)_2]_n$ tube-like chain, which further expanded to the 6-connected $(4^8\cdot6^7)$ network. For complex **2**, the coordination mode is simple, the bridging bifunctional $Hbcb^{2-}$ interact with Cd^{II} ions formed a 2D $[Cd(Hbcb)]_n$ layer, and the neighbouring 2D layers are further interact with each other though the hydrogen bonds between protonated carboxyl groups and the deprotonated ones of different sheets. Then, the 2D $[Cd(Hbcb)]_n$ layers are further expanded along the 1D $[Cd(1,4\text{-bib})]_n$ chains direction, given a

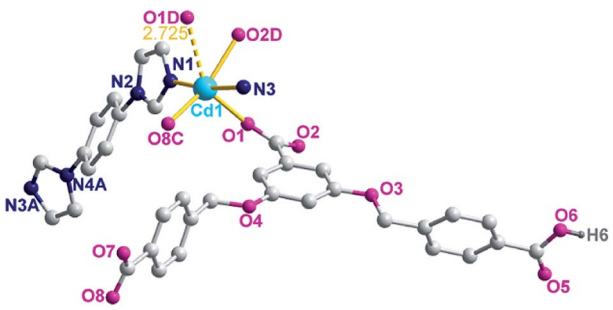

Fig. 5 ORTEP representation of **2** showing the local coordination environment around Cd^{II} center. (Symmetry codes: (A) *x*, −*y*, −0.5 + *z*; (C) 1 − *x*, −1 − *y*, 2 − *z*; (D) 1.5 − *x*, −0.5 + *y*, *z*.).

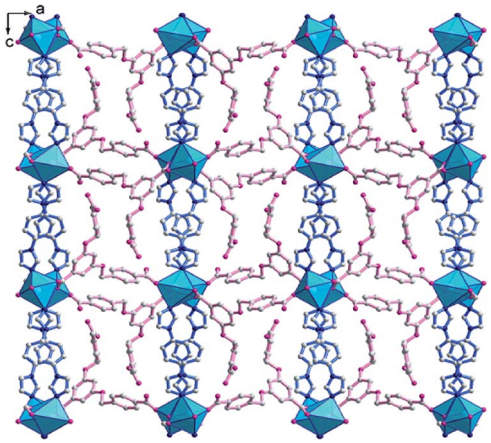

Fig. 6 View of the 3D frameworks in complex **2**.

3D (3,5)-connected framework finally. The 1,4-bib ligand in complex **2** was thought act as a pillar to support adjacent $[Cd(Hbcb)]_n$ layers. The structural differences indicated the co-ligand of 1,4-bib has great influences on the coordination modes of H_3bcb and the packing structure due to that the stereospecific blockade of 1,4-bib make $Hbcbb^{2-}$ extremely unsymmetrical and distorted during the self-assembly process. Thence, when the 1,4-bib ancillary ligand were added in construction of CPs, the polycarboxylates tend to connect with fewer metal ions (the change of coordination modes), and adjust themselves to satisfy the needs of lowest system energy by twisting, rotating, and folding, further effect the final structure. It is also noteworthy that the protonated carboxyl group on the benzyl ring in complexes **1–4** shows that three carboxyl groups in H_3bcb have different acidity.

X-ray podwer diffraction analyses and thermal analyses

Powder X-ray diffraction (XRD) has been used to check the phase purity of the bulky samples in the solid state. For complexes **1–4**, the measured XRD patterns are closely identical to the simulated patterns generated from the results of single-crystal diffraction data by Mercury program,[17] indicative of pure products (Fig. S4, ESI†). The thermogravimetric (TG) analyses on polycrystalline samples of complexes **1–4** were performed in N_2 atmosphere and the TG curves are shown in Fig. S5.† For complex **1**, the whole structure is stable below 425 °C, and then the framework collapses with a result of thermal decomposition. For complexes **2–4**, the water-free networks are stable below 350 °C, 370 °C, and 340 °C, respectively.

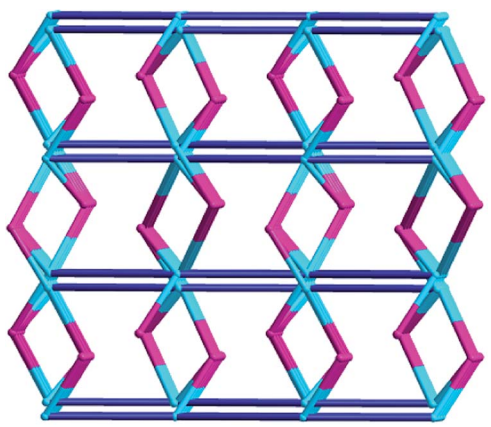

Fig. 7 Schematic view of the novel binodal (3,5)-connected $(4\cdot6\cdot8)(4\cdot6^4\cdot8^5)$ topology of complex **2**.

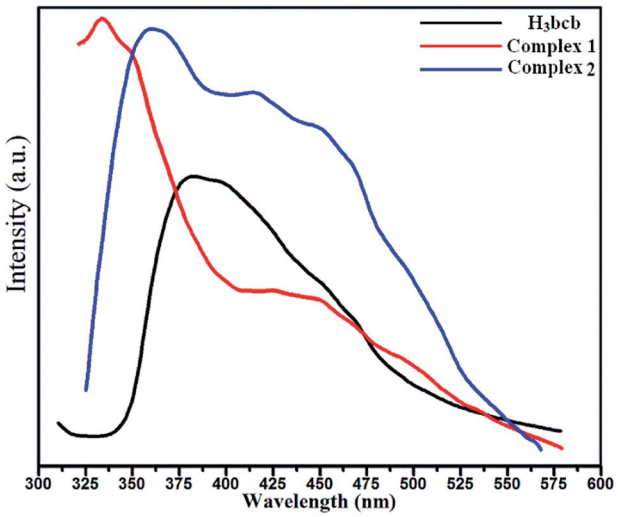

Fig. 8 Solid-state emission spectra of H_3bcb ligand and the complexes **1** and **2** at room temperature.

Photoluminescent investigation

The photoluminescent properties of H_3bcb and complexes **1** and **2** have been investigated under 300 nm wavelength excitation at room temperature, and the normalised photoluminescent spectres were shown in Fig. 8. For the ligand H_3bcb, the main peak at 383 nm can be attributed to the $\pi^* \rightarrow$ n or $\pi^* \rightarrow \pi$ transitions. The emission spectra for **1** and **2** exhibit emission peaks of 334 and 361 nm, respectively, which may be assigned to the intraligand emission ($\pi^* \rightarrow$ n or $\pi^* \rightarrow \pi$). These emissions are neither metal-to-ligand charge transfer (MLCT) nor ligand-to-metal transfer (LMCT) in nature since the Cd^{II} ion is difficult to oxidize or reduce due to its d^{10} configuration.[18] The blue-shifted results of the Cd^{II}-containing complexes can be attributed to the H_3bcb ligand conformational change after dehydrogenation, which make the conjugated system reduced.[19] The difference of the emission behaviours for complexes **1** and **2** probably derive from the differences of solid-state crystal packing.

Conclusions

In summary, with the elaborately designed flexible and longer ligand of 3,5-bis((4′-carboxylbenzyl)oxy)benzoic acid (H_3bcb), four new complexes with undocumented topologies were obtained. When the 1,4-bib ancillary ligand was introduced into the reaction, a structural transformation from 6-connected $(4^8\cdot6^7)$ to (3,5)-connected $(4\cdot6\cdot8)(4\cdot6^4\cdot8^5)$ took place. The result

demonstrated that the employment of the ancillary 1,4-bib linker in the assembly of metal–polycarboxylates coordination polymers could lead to structural changes and unprecedented topologies since the stereospecific blockade of 1,4-bib make $Hbcbb^{2-}$ extremely unsymmetrical and distorted during the self-assembly process.

This will be the subject of future studies in our lab.

Conflict of interest

The authors declare no competing financial interest.

Acknowledgements

The work was supported by financial support from the Natural Science Foundation of China (grant nos. 21101097, 91022034 and 51172127), the Excellent Youth Foundation of Shandong Scientific Committee (Grant JQ201015).

References

1 (*a*) G. Férey and C. Serre, *Chem. Soc. Rev.*, 2009, **38**, 1380; (*b*) H. Fei, J. F. Cahill, K. A. Prather and S. M. Cohen, *Inorg. Chem.*, 2013, **52**, 4011; (*c*) M. O'Keeffe and O. M. Yaghi, *Chem. Rev.*, 2011, **112**, 675; (*d*) M. D. Allendorf, C. A. Bauer, R. K. Bhakata and R. J. T. Houk, *Chem. Soc. Rev.*, 2009, **38**, 1330.

2 (*a*) J. Duan, M. Higuchi, R. Krishna, T. Kiyonaga, Y. Tsutsumi, Y. Sato, Y. Kubota, M. Takata and S. Kitagawa, *Chem. Sci.*, 2014, **5**, 660; (*b*) M. Zhang, W. Lu, J. R. Li, M. Bosch, Y. P. Chen, T. F. Liu, Y. Liu and H. C. Zhou, *Inorg. Chem. Front.*, 2014, **1**, 159; (*c*) B. L. Chen, N. W. Ockwig, A. R. Millward, D. S. Contreras and O. M. Yaghi, *Angew. Chem., Int. Ed.*, 2005, **44**, 4745; (*d*) A. B. Canaj, L. F. Nodaraki, K. Slepokura, M. Siczek, D. I. Tzimopoulos, T. Lis and C. J. Milios, *RSC Adv.*, 2014, **4**, 23068.

3 (*a*) E. D. Bloch, W. L. Queen, R. Krishna, J. M. Zadrozny, C. M. Brown and J. R. Long, *Science*, 2012, **335**, 1606; (*b*) T. B. Saust and D. M. D'Alessandro, *RSC Adv.*, 2014, **4**, 17498; (*c*) L. J. Murray, M. Dincâ and J. R. Long, *Chem. Soc. Rev.*, 2009, **38**, 1294; (*d*) X. Zhang, L. Fan, W. Zhang, Y. Ding, W. Fan and X. Zhao, *Dalton Trans.*, 2013, **42**, 16562; (*e*) M. H. Weston, A. A. Delaquil, A. A. Sarjeant, O. K. Farha, J. T. Hupp and S. T. Nguyen, *Cryst. Growth Des.*, 2013, **13**, 2938.

4 (*a*) P. V. Dau and S. M. Cohen, *Chem. Commun.*, 2013, **49**, 6128; (*b*) X. T. Zhang, D. Sun, B. Li, L. M. Fan, B. Li and P. H. Wei, *Cryst. Growth Des.*, 2012, **12**, 3845; (*c*) T. Ishimoto, T. Ogura, M. Koyama, L. F. Yang, S. Kinoshita, T. Yamada, M. Tokunaga and H. Kitagawa, *J. Phys. Chem. C*, 2013, **117**, 10607; (*d*) J. Y. Zou, W. Shi, H. L. Gao, J. Z. Cui and P. Cheng, *Inorg. Chem. Front.*, 2014, **1**, 242.

5 (*a*) S. Chen, R. Shang, K. L. Hu, Z. M. Wang and S. Gao, *Inorg. Chem. Front.*, 2014, **1**, 83; (*b*) S. Kennedy, I. E. Dodgson, C. M. Beavers, S. J. Teat and S. J. Dalgarno, *Cryst. Growth Des.*, 2012, **12**, 688; (*c*) T. Devic, P. Horcajada, C. Serre, F. Salles, G. Maurin, B. Moulin, D. Heurtaux, G. Clet, A. Vimont, J. M. Grenèche, B. LeOuay, F. Moreau, E. Magnier, Y. Filinchuk, J. Marrot, J. C. Lavalley, M. Daturi and G. Férey, *J. Am. Chem. Soc.*, 2010, **132**, 1127; (*d*) X. T. Zhang, L. M. Fan, X. Zhao, D. Sun, D. C. Li and J. M. Dou, *CrystEngComm*, 2012, **14**, 2053.

6 (*a*) R. Krishna and J. M. van Baten, *J. Phys. Chem. C*, 2010, **114**, 18017; (*b*) D. X. Xue, A. J. Cairns, Y. Belmabkhout, L. Wojtas, Y. L. Liu, M. H. Alkordi and M. Eddaoudi, *J. Am. Chem. Soc.*, 2013, **135**, 7660; (*c*) D. Sun, L. L. Han, S. Yuan, Y. K. Deng, M. Z. Xu and D. F. Sun, *Cryst. Growth Des.*, 2013, **13**, 377; (*d*) X. Zhang, L. Fan, Z. Sun, W. Zhang, W. Fan, L. Sun and X. Zhao, *CrystEngComm*, 2013, **15**, 4910.

7 (*a*) X. H. Chang, J. H. Qin, M. L. Han, L. F. Ma and L. Y. Han, *CrystEngComm*, 2014, **16**, 870; (*b*) G. A. Senchyk, A. B. Lysenko, H. Krautscheid, E. B. Rusanov, A. N. Chernega, K. W. Krämer, S. X. Liu, S. Decurtins and K. V. Domasevitch, *Inorg. Chem.*, 2013, **52**, 863; (*c*) V. Kulikov and G. Meyer, *Cryst. Growth Des.*, 2013, **13**, 2916; (*d*) L. Fan, X. Zhang, D. Li, D. Sun, W. Zhang and J. Dou, *CrystEngComm*, 2013, **15**, 349.

8 (*a*) M. Kim, J. F. Cahill, H. Fei, K. A. Prather and S. M. Cohen, *J. Am. Chem. Soc.*, 2012, **134**, 18082; (*b*) Y. B. Wang, Y. L. Lei, S. H. Chi and Y. J. Luo, *Dalton Trans.*, 2013, **42**, 1862; (*c*) O. K. Farha, A. M. Shultz, A. A. Sarjeant, S. T. Nguyen and J. T. Hupp, *J. Am. Chem. Soc.*, 2011, **133**, 5652; (*d*) X. Zhang, L. Fan, Z. Sun, W. Zhang, D. Li, J. Dou and L. Han, *Cryst. Growth Des.*, 2013, **13**, 792.

9 (*a*) D. L. Long, R. Tsunashima and L. Cronin, *Angew. Chem., Int. Ed.*, 2010, **49**, 1736; (*b*) M. W. Schneider, H. J. S. Hauswald, R. Stoll and M. Mastalerz, *Chem. Commun.*, 2012, **48**, 9861; (*c*) L. Fan, Y. Gao, G. Liu, W. Fan, W. Song, L. Sun, X. Zhao and X. Zhang, *CrystEngComm*, 2014, DOI: 10.1039/C4CE00760C.

10 (*a*) T. Hasell, M. Schmidtmann, C. A. Stone, M. W. Smith and A. I. Cooper, *Chem. Commun.*, 2012, **48**, 4689; (*b*) Q. L. Zhang, G. W. Feng, Y. Q. Zhang and B. X. Zhu, *RSC Adv.*, 2014, **4**, 11384; (*c*) R. P. Davies, R. Less, P. D. Lickiss, K. Robertson and A. J. P. White, *Cryst. Growth Des.*, 2010, **10**, 4571; (*d*) Q. L. Zhang, P. Hu, Y. Zhao, G. W. Feng, Y. Q. Zhang, B. X. Zhu and Z. Tao, *J. Solid State Chem.*, 2014, **210**, 178.

11 (*a*) S. T. Zheng, H. Zhang and G. Y. Yang, *Angew. Chem., Int. Ed.*, 2008, **47**, 3909; (*b*) Y. Kikukawa, K. Yamaguchi and N. Mizuno, *Angew. Chem., Int. Ed.*, 2010, **49**, 6096; (*c*) L. Fan, X. Zhang, W. Zhang, Y. Ding, W. Fan, L. Sun, Y. Pang and X. Zhao, *Dalton Trans.*, 2014, **43**, 6701; (*d*) B. Liu, L. Wei, N. N. Li, W. P. Wu, H. Miao, Y. Y. Wang and Q. Z. Shi, *Cryst. Growth Des.*, 2014, **14**, 1110.

12 (*a*) P. Lama, J. Mrozinski and P. K. Bharadwaj, *Cryst. Growth Des.*, 2012, **12**, 3158; (*b*) Y. Zhang, J. Yang, Y. Yang, J. Guo and J. F. Ma, *Cryst. Growth Des.*, 2012, **12**, 4060; (*c*) M. Ahmad, R. Das, P. Lama, P. Poddar and P. K. Bharadwaj, *Cryst. Growth Des.*, 2012, **12**, 4624.

13 (*a*) L. Fan, X. Zhang, Z. Sun, W. Zhang, Y. Ding, W. Fan, L. Sun, X. Zhao and H. Lei, *Cryst. Growth Des.*, 2013, **13**, 2462; (*b*) F. Guo, B. Zhu, M. Liu, X. Zhang, J. Zhang and J. Zhao, *CrystEngComm*, 2013, **15**, 6191; (*c*) X. Zhang,

L. Fan, W. Zhang, W. Fan, L. Sun and X. Zhao, *CrystEngComm*, 2014, **16**, 3203.

14 (*a*) G. M. Sheldrick, *SHELXTL, version 5.1*; Bruker Analytical X-ray Instruments Inc., Madison, WI, 1998; (*b*) G. M. Sheldrick, *SHELX-97, PC Version*; University of Gottingen: Gottingen, Germany, 1997.

15 (*a*) V. A. Blatov, A. P. Shevchenko and V. N. Serezhkin, *J. Appl. Crystallogr.*, 2000, **33**, 1193; (*b*) The network topology was evaluated by the program "TOPOS-4.0", see: http://www.topos.ssu.samara.ru; (*c*) V. A. Blatov, M. O'Keeffe and D. M. Proserpio, *CrystEngComm*, 2010, **12**, 44.

16 (*a*) A. L. Spek, *J. Appl. Crystallogr.*, 2003, **36**, 7; (*b*) A. L. Spek, *PLATON, A Multipurpose Crystallographic Tool*, Utrecht University, Utrecht, The Netherlands, 2002.

17 C. F. Macrae, P. R. Edgington, P. McCabe, E. Pidcock, G. P. Shields, R. Taylor, M. Towler and J. V. D. Streek, *J. Appl. Crystallogr.*, 2006, **39**, 453.

18 (*a*) L. Zhu, Z. Yuan, J. T. Simmons and K. Sreenath, *RSC Adv.*, 2014, **4**, 20398; (*b*) J. Liu, H. B. Zhang, Y. X. Tan, F. Wang, Y. Kang and J. Zhang, *Inorg. Chem.*, 2014, **53**, 1500; (*c*) Y. Cui, Y. Yue, G. Qian and B. Chen, *Chem. Rev.*, 2012, **112**, 1126.

19 (*a*) V. Kumar, V. Singh, A. N. Gupta, K. K. Manar, G. B. Drew and N. Singh, *CrystEngComm*, 2014, **16**, 6765; (*b*) P. C. Cheng, P. T. Kuo, Y. H. Liao, M. Y. Xie, W. Hsu and J. D. Chen, *Cryst. Growth Des.*, 2013, **13**, 623; (*c*) D. Sun, S. Yuan, H. Wang, H. F. Lu, S. Y. Feng and D. F. Sun, *Chem. Commun.*, 2013, **49**, 6152.